Supplementary Information

Secondary Organic Aerosol Formation from Nitrate Radical Oxidation of Styrene: Aerosol Yields, Chemical Composition, and Hydrolysis of Organic Nitrates

Yuchen Wang[1,2], Xiang Zhang[1], Yuanlong Huang[3], Yutong Liang[2,6], Nga L. Ng*[,2,4,5]

[1] College of Environmental Science and Engineering, Hunan University, Changsha, Hunan, 410082, China

[2] School of Chemical and Bimolecular Engineering, Georgia Institute of Technology, Atlanta, Georgia 30332, USA

[3] Ningbo Institute of Digital Twin, Eastern Institute of Technology, Ningbo, 315200, China

[4] School of Civil and Environmental Engineering, Georgia Institute of Technology, Atlanta, Georgia 30332, USA

[5] School of Earth and Atmospheric Sciences, Georgia Institute of Technology, Atlanta, Georgia 30332, USA

[6] Thrust of Sustainable Energy and Environment, The Hong Kong University of Science and Technology (Guangzhou), Guangdong, 511453, China

*Corresponding Author: Nga Lee Ng (ng@chbe.gatech.edu)

This supplemental information contains 2 tables and 9 figures, totaling 16 pages including the cover page.
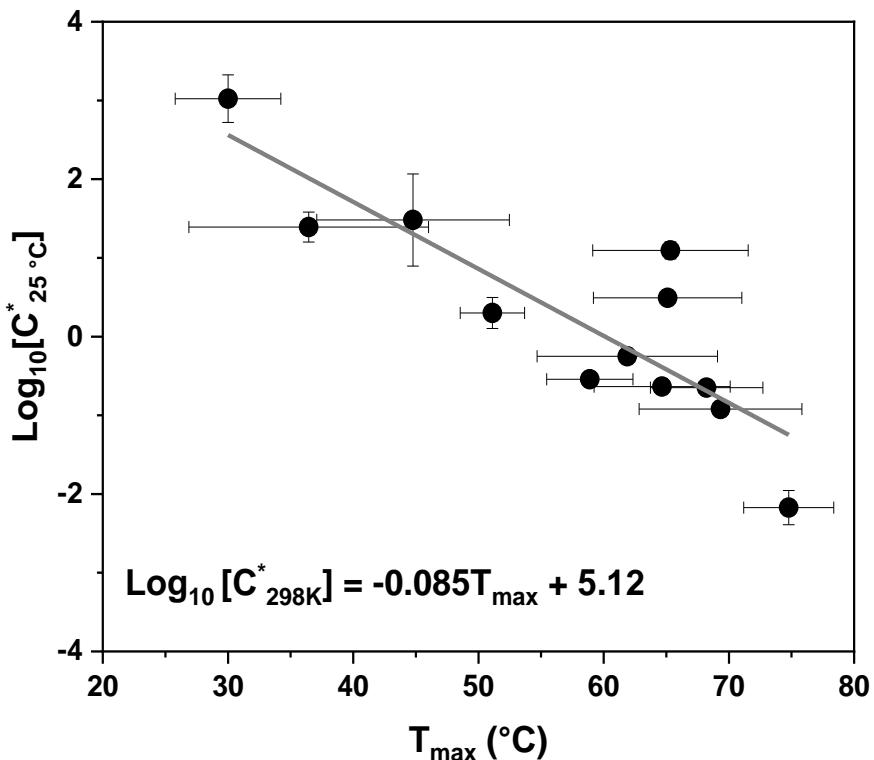
23
24 **Figure S1**. Volatility calibration curve of a filter inlet for gases and aerosols coupled to a chemical
25 ionization mass spectrometer (FIGAERO-CIMS). Filled circles and error bars are mean values and standard
26 deviation of two calibrations, respectively. The line represents a total least-squares fit. These results are
27 comparable to those reported in Takeuchi et al. (2022).
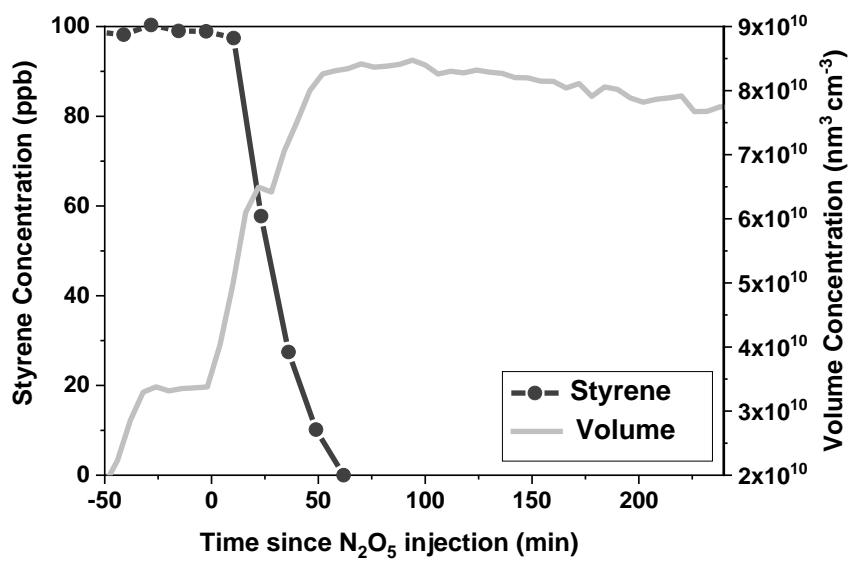
28
29 **Figure S2**. Typical time profile of the decay of styrene over time measured by GC-FID and aerosol
30 fromation (volume concentration) measued by SMPS, particle wall loss corrected (Exp. 7).

31
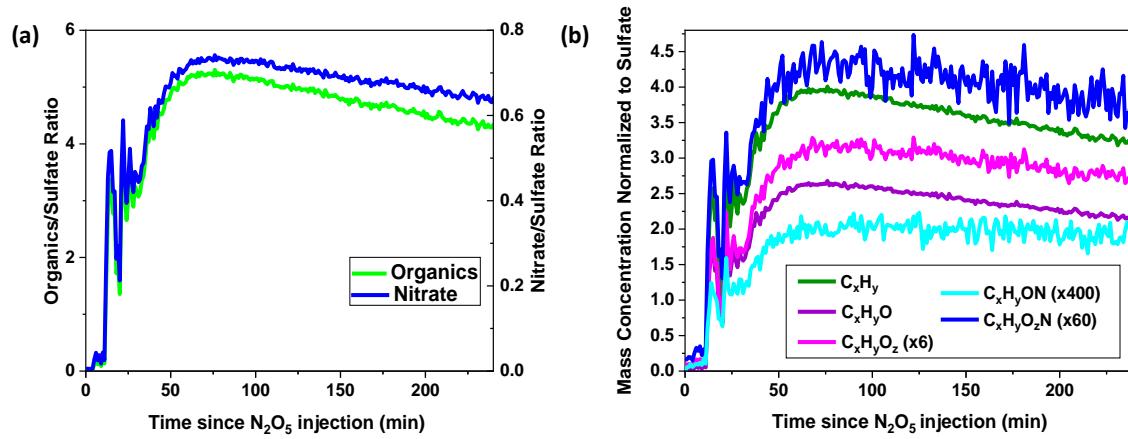
32

33 **Figure S3**. (a) Time series of mass concentrations of organics and nitrate (normalized to the sulfate mass

34 concentration); (b) Time series of mass concentrations of C_xH_y, C_xH_yO, $C_xH_yO_z$, C_xH_yON, and $C_xH_yO_zN$

35 families (normalized to the sulfate mass concentration) measured by HR-ToF-AMS (Exp.7).
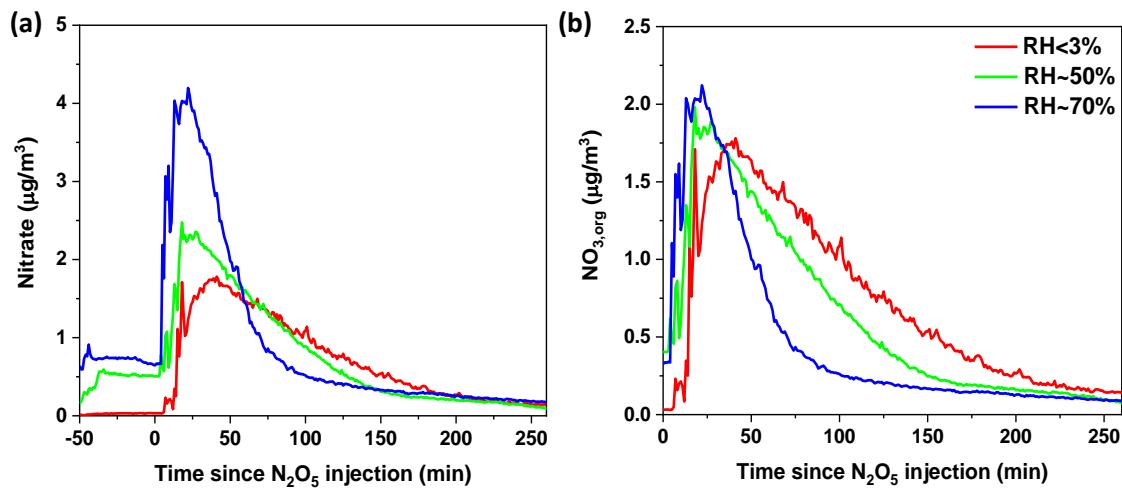
36
37 **Figure S4**. Time series of (a) nitrate measured by HR-ToF-AMS and (b) organic nitrates ($NO_{3,org}$) from
38 Exp. 2 (RH<3%), Exp. 11 (RH~50%), and Exp. 12 (RH~70%).
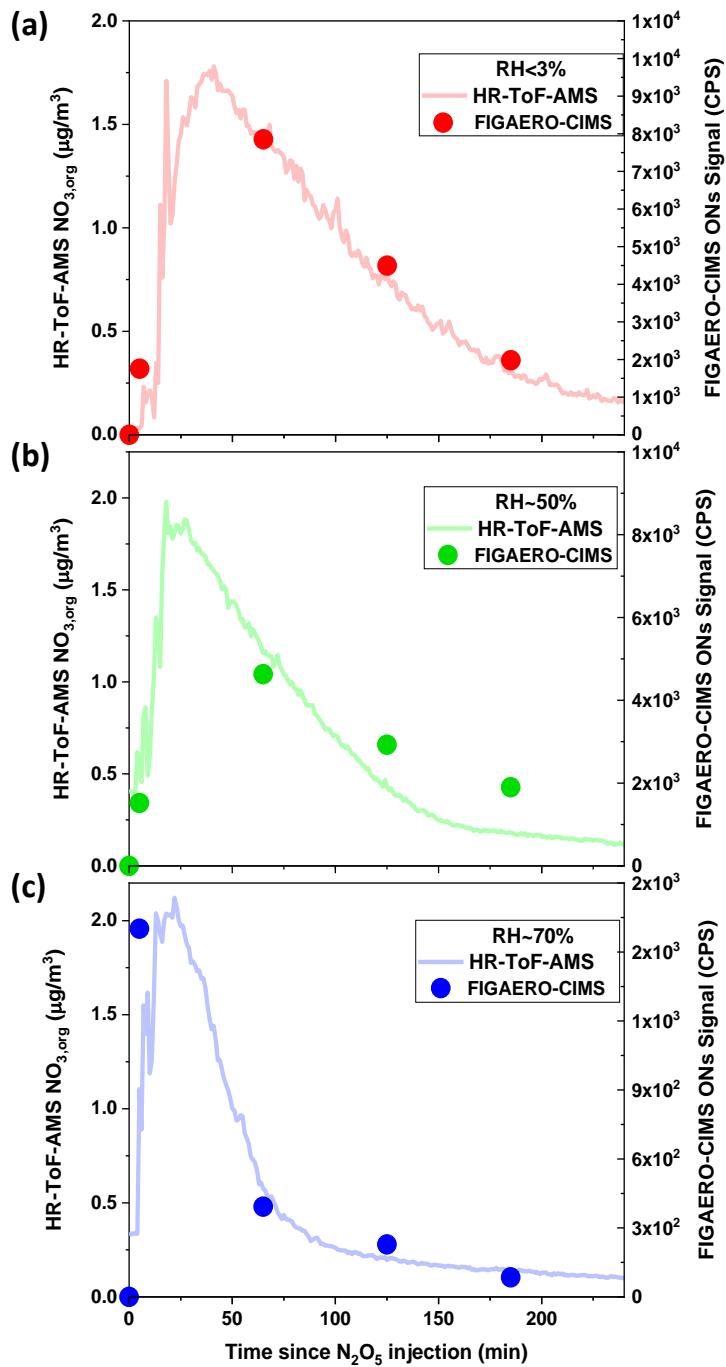
39

40 **Figure S5.** Time series of organic nitrates ($NO_{3,org}$) measured by HR-ToF-AMS and the sum of ON signals

41 measured by FIGAERO-CIMS: (a) RH<3% (Exp.2); (b) RH~50% (Exp.11); and (c) RH~70% (Exp. 12).
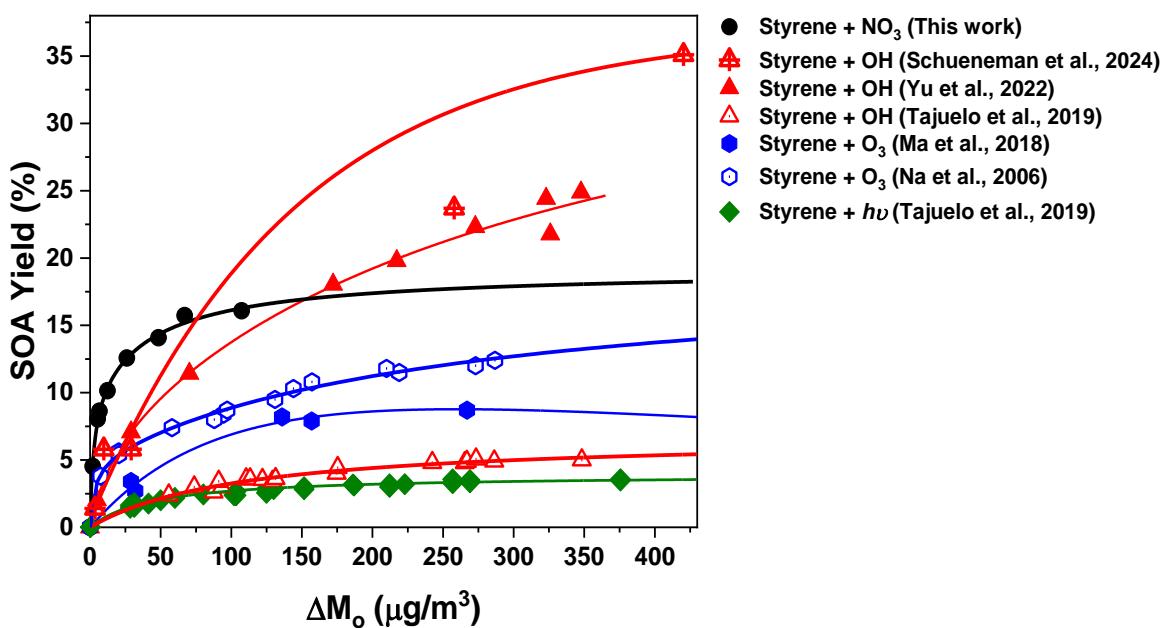
42
43 **Figure S6**. Comparison of SOA yields of styrene oxidation systems in this work and in literature (Yu et al.,

44 2022; Tajuelo et al., 2019; Ma et al., 2018; Na et al., 2006; Schueneman et al., 2024). The SOA yields and

45 ΔM_O in Schueneman et al., (2024) and in Tajuelo et al., (2019) are extracted by WebPlotDigitizer.
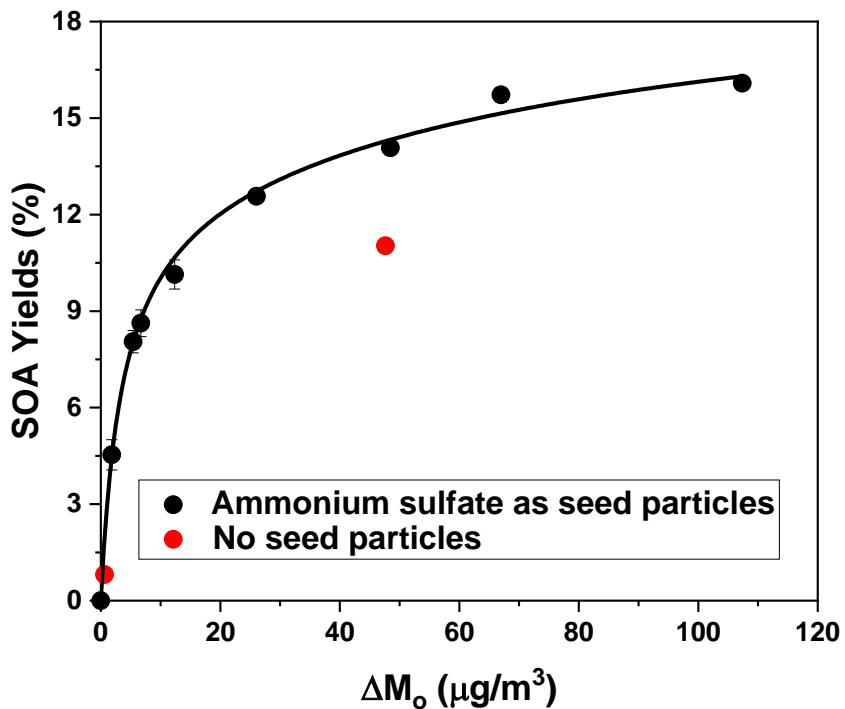
46
47   **Figure S7.** SOA yields of styrene+NO$_3$ oxidation: with seed particles (filled circles; fitted to yield curve)

48   and without any seed particles (red dots for Exp. 9 and 10).

Accounting for vapor wall loss in determining SOA yields

To evaluate the potential effect of organic vapor wall loss on SOA yields in our study, experiments without seed particles are carried out. As shown in Figure S7, the SOA formation from nucleation experiments (without seed particles) are lower than condensation experiments (with seed particles). We employ the semi-empirical equation based on gas-to-particle partitioning of two semi-volatile products (Odum et al., 1996, 1997) for SOA yields to correct for vapor wall loss in SOA yield determination (Eq. S1).

$$Y = \Delta M_O [\frac{\alpha_1 K_1}{1+K_1 M_O} + \frac{\alpha_2 K_2}{1+K_2 M_O}] \qquad \text{Eq. S1}$$

Where Y is the SOA yield, M_O is the aerosol mass loading, α_1 and α_2 are the fitted molar yields of the two products, and K_1 and K_2 are the fitted partitioning coefficients of the two products. K is inversely proportional to the saturation mass concentration (C*) of each pure semi-volatile compound. The correction relies on the assumption that styrene+NO_3 oxidation yields two major products. After correcting for particle wall loss, the total mass of products (C) can reside in three components: in the gas phase (C_g), in the particle phase (C_p), and on the chamber wall (C_w) due to vapor wall loss. In the two-product semi-empirical model, the term α represents the fitted molar yield. Therefore, the total mass concentration of products can also be expressed as the products of the fitted molar yield and the amount of styrene reacted (ΔHC) as shown in Eq. S2 and S3.

$$C_g^1 + C_p^1 + C_w^1 = \Delta\text{HC} \times \alpha_1 \qquad \text{Eq. S2}$$

$$C_g^2 + C_p^2 + C_w^2 = \Delta\text{HC} \times \alpha_2 \qquad \text{Eq. S3}$$

According to the two-layer model in Huang et al., (2018), the vapor wall loss is the overall decay of vapor molecules in the surface and inner layers of the chamber wall after equilibrium (Eq. S4). As shown in Eq. S5 and S6, C_w can be calculated from C_g, activity coefficient in Teflon film (r_1^∞), C*, and equivalent total wall concentration (C_{TW}, sum of C_w^1 and C_w^2).

$$C_{TW} = \frac{10.8*A}{V} \qquad \text{Eq. S4}$$

$$C_g^1 = C_1^* \times r_1^\infty \times \frac{C_w^1}{C_{TW}} = C_1^* \times 10^{3.299} \times (C_1^*)^{-0.6407} \times \frac{C_w^1}{\frac{10.8*A}{V}} \qquad \text{Eq. S5}$$

$$C_g^2 = C_2^* \times r_2^\infty \times \frac{C_w^2}{C_{TW}} = C_2^* \times 10^{3.299} \times (C_2^*)^{-0.6407} \times \frac{C_w^2}{\frac{10.8*A}{V}} \qquad \text{Eq. S6}$$

Where A refers to the chamber surface area (m^2) and V refers to chamber volume (m^3).

According to previous work (Pankow, 1994a, b), C_g can be calculated from C_p, C*, and M_O (Eq. S7 and S8).

$$C_g^1 = C_1^* \times \frac{C_p^1}{M_O} \qquad \text{Eq. S7}$$

79
$$C_g^2 = C_2^* \times \frac{C_p^2}{M_O}$$
Eq. S8

80   Therefore, Eq. S2 and S3 can be rewritten to Eq. S9 and S10, respectively:

81
$$C_1^* \times \frac{C_p^1}{M_O} + C_p^1 + \frac{C_p^1 \times C_{TW}}{M_O \times r_1^\infty} = \Delta HC \times \alpha_1$$
Eq. S9

82
$$C_2^* \times \frac{C_p^2}{M_O} + C_p^2 + \frac{C_p^2 \times C_{TW}}{M_O \times r_2^\infty} = \Delta HC \times \alpha_2$$
Eq. S10

83   The two-product semi-empirical model (Eq. S1) can also be rewritten to Eq. S11:

84
$$Y = \frac{\Delta M_O}{\Delta HC} = \frac{C_p^1 + C_p^2}{\Delta HC} = \frac{\frac{\Delta HC \times \alpha_1}{C_1^* \times \frac{1}{M_O} + 1 + \frac{C_{TW}}{M_O \times r_1^\infty}} + \frac{\Delta HC \times \alpha_2}{C_2^* \times \frac{1}{M_O} + 1 + \frac{C_{TW}}{M_O \times r_2^\infty}}}{\Delta HC} = \Delta M_O \left[\frac{\alpha_1 K_1}{1 + K_1 M_O + \frac{K_1 \times C_{TW}}{r_1^\infty}} + \frac{\alpha_2 K_2}{1 + K_2 M_O + \frac{K_2 \times C_{TW}}{r_2^\infty}} \right]$$

85
Eq. S11

86   The ΔM_O and SOA yields after the correction are shown in Table S1. SOA yield curve after the

87   correction is shown in Figure 1. The fitted molar yields (α_1 and α_2) are 0.84 and 0.14, and the fitted

88   partitioning coefficients (K_1 and K_2) are 8.08×10^{-4} and 7.48 after vapor wall loss correction ($R^2 = 0.991$).

89

90 **Table S1**. SOA yield data for styrene+NO_3 oxidation with and without vapor wall loss correction.

Exp	ΔM_O (μg m^{-3})	Corrected ΔM_O (μg m^{-3})	SOA Mass yield (%)	Corrected SOA Mass yield (%)
1	1.9	5.9	4.5	14.5
2	5.4	9.6	8.1	14.3
3	6.8	11	8.6	14.2
4	12.4	17.1	10.1	14.0
5	26.1	32.5	12.6	15.7
6	48.5	60.2	14.1	17.5
7	67.0	85.4	15.7	20.0
8	107.4	147.6	16.1	22.1

91

92
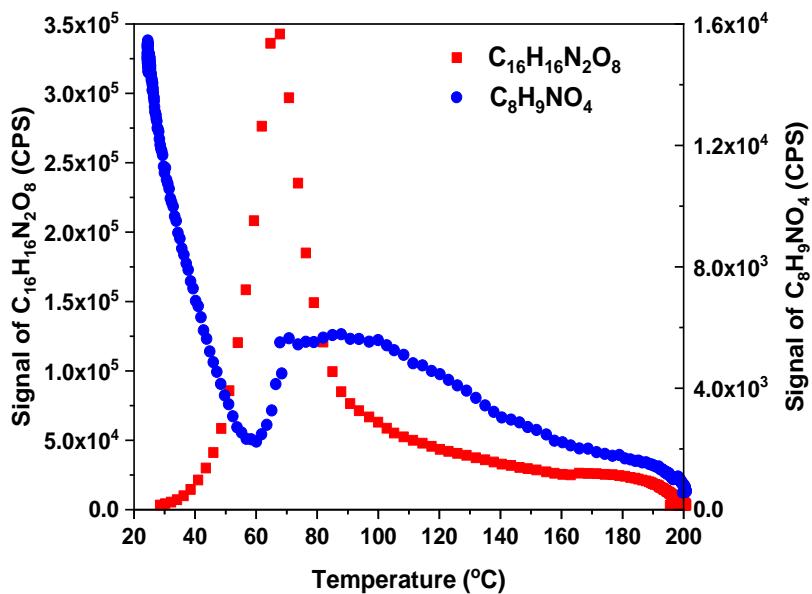
93
94 **Figure S8.** Thermal desorption profiles of $C_{16}H_{16}N_2O_8$ and $C_8H_9NO_4$ in FIGAERO-CIMS from Exp. 7.

95 Data points are averages of three desorption cycles around the time of the peak SOA mass concentration.

Pathway C: Proposed Mechanisms for ONs Formation from Nitrooxy Peroxy Radical Isomer
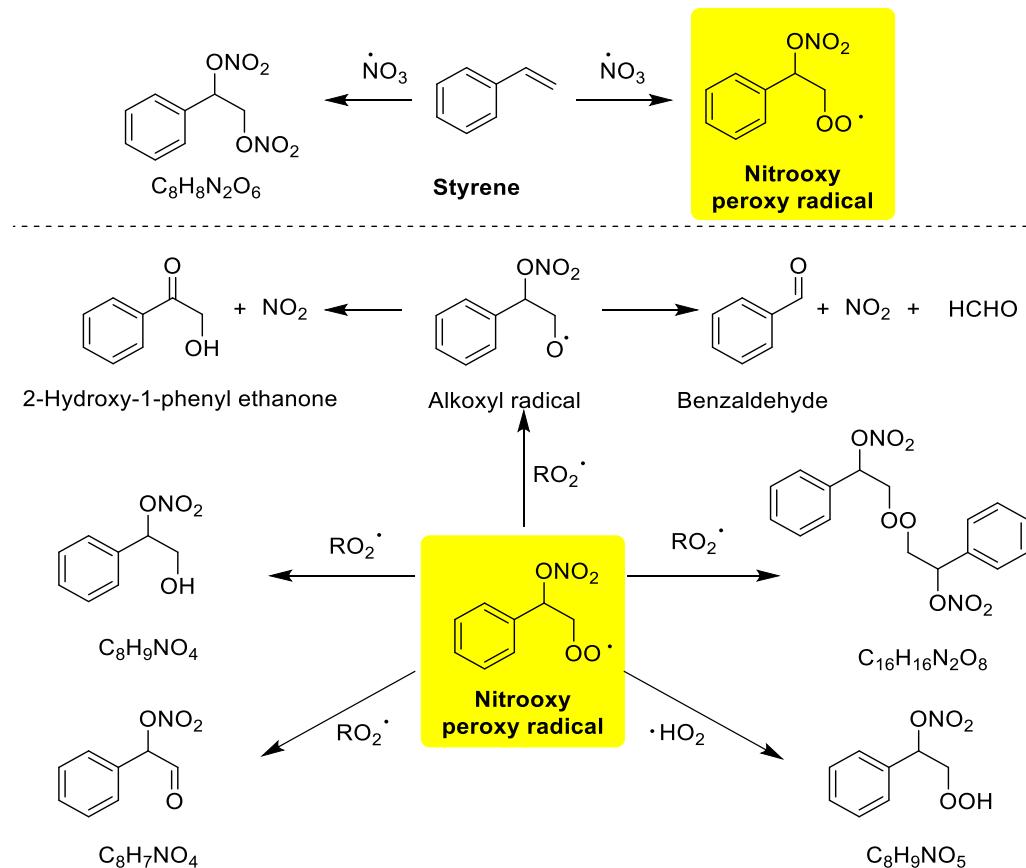
Figure S9. Proposed mechanisms for the major particle-phase products resulting from further reactions of the nitrooxy peroxy radcial. The nitrooxy peroxy radical is highlighted in yellow as the major RO_2 in the mechanisms.

Table S2. Possible dimeric aromatic ONs measured by FIGAERO-CIMS in ambient studies.

Molecular Formula[a]	Molecular Weight	RDBE[b]	Xc[c]
$C_{20}H_{21}NO_5$	354.142	11	2.78
$C_{20}H_{23}NO_5$	356.1576	10	2.75
$C_{20}H_{21}NO_6$	370.1369	11	2.75
$C_{20}H_{23}NO_6$	372.1525	10	2.71
$C_{20}H_{21}NO_7$	386.1318	11	2.71
$C_{20}H_{22}N_2O_7$	401.1427	11	2.80
$C_{19}H_{22}N_2O_8$	405.1376	10	2.75
$C_{20}H_{20}N_2O_8$	415.1219	11	2.78
$C_{20}H_{22}N_2O_8$	417.1376	11	2.78
$C_{20}H_{24}N_2O_8$	419.1533	10	2.75
$C_{19}H_{22}N_2O_9$	421.1325	10	2.71
$C_{22}H_{26}N_2O_7$	429.174	11	2.80
$C_{20}H_{22}N_2O_9$	433.1325	11	2.75
$C_{20}H_{24}N_2O_9$	435.1482	10	2.71
$C_{22}H_{26}N_2O_8$	445.1689	11	2.78
$C_{20}H_{22}N_2O_{10}$	449.1274	11	2.71
$C_{22}H_{26}N_2O_9$	461.1638	11	2.75

[a.] The molecular formula are obtained from a field campaign conducted in Shenzhen, China, using FIGAERO-CIMS. (Ye et al., 2021) [b.] RDBE is ring and double-bond equivalence. $RDBE = \frac{Carbon\ number \times 2 + 2 - Hydrogen\ number + Nitrogen\ number}{2}$. [c.] Xc is aromaticity equivalent. $Xc = \frac{3 \times (RDBE - (Oxygen\ number - 3 \times Nitrogen\ number)) - 2}{RDBE - (Oxygen\ number - 3 \times Nitrogen\ number)}$. The aromaticity equivalent equation, as discussed by Yassine et al. (2014) and Wang et al. (2017), has been revised based on the assumption that the nitrooxy group requires three oxygen atoms.

References:

Huang, Y., Zhao, R., Charan, S. M., Kenseth, C. M., Zhang, X., and Seinfeld, J. H.: Unified Theory of Vapor-Wall Mass Transport in Teflon-Walled Environmental Chambers, Environ. Sci. Technol., 52, 2134–2142, https://doi.org/10.1021/acs.est.7b05575, 2018.

Kroll, J. H. and Seinfeld, J. H.: Chemistry of secondary organic aerosol: Formation and evolution of low-volatility organics in the atmosphere, Atmos. Environ., 42, 3593–3624, https://doi.org/10.1016/j.atmosenv.2008.01.003, 2008.

Ma, Q., Lin, X., Yang, C., Long, B., Gai, Y., and Zhang, W.: The influences of ammonia on aerosol formation in the ozonolysis of styrene: Roles of criegee intermediate reactions, R. Soc. Open Sci., 5, 172171–172183, https://doi.org/10.1098/rsos.172171, 2018.

Na, K., Song, C., and Cocker, D. R.: Formation of secondary organic aerosol from the reaction of styrene with ozone in the presence and absence of ammonia and water, Atmos. Environ., 40, 1889–1900, https://doi.org/10.1016/j.atmosenv.2005.10.063, 2006.

Odum, J. R., Hoffmann, T., Bowman, F., Collins, D., Flagan, R. C., and Seinfeld, J. H.: Gas/particle partitioning and secondary organic aerosol yields, Environ. Sci. Technol., 30, 2580–2585, https://doi.org/10.1021/es950943+, 1996.

Odum, J. R., Jungkamp, T. P. W., Griffin, R. J., Flagan, R. C., and Seinfeld, J. H.: The Atmospheric Aerosol-Forming Potential of Whole Gasoline Vapor, Science (80-.)., 276, 96–99, https://doi.org/10.1126/science.276.5309.96, 1997.

Pankow, J. F.: An absorption model of gas/particle partitioning of organic compounds in the atmosphere, Atmos. Environ., 28, 185–188, https://doi.org/https://doi.org/10.1016/1352-2310(94)90093-0, 1994a.

Pankow, J. F.: An absorption model of the gas/aerosol partitioning involved in the formation of secondary organic aerosol, Atmos. Environ., 28, 189–193, https://doi.org/https://doi.org/10.1016/1352-2310(94)90094-9, 1994b.

Schueneman, M. K., Day, D. A., Peng, Z., Pagonis, D., Jenks, O. J., de Gouw, J. A., and Jimenez, J. L.: Secondary Organic Aerosol Formation from the OH Oxidation of Phenol, Catechol, Styrene, Furfural, and Methyl Furfural, ACS Earth Sp. Chem., 8, 1179–1192, https://doi.org/10.1021/acsearthspacechem.3c00361, 2024.

Tajuelo, M., Rodríguez, D., Baeza-Romero, M. T., Díaz-de-Mera, Y., Aranda, A., and Rodríguez, A.: Secondary organic aerosol formation from styrene photolysis and photooxidation with hydroxyl radicals, Chemosphere, 231, 276–286, https://doi.org/10.1016/j.chemosphere.2019.05.136, 2019.

Takeuchi, M., Berkemeier, T., Eris, G., and Ng, N. L.: Non-linear effects of secondary organic aerosol formation and properties in multi-precursor systems, Nat. Commun., 13, 1–13, https://doi.org/10.1038/s41467-022-35546-1, 2022.

140   Wang, X., Hayeck, N., Brüggemann, M., Yao, L., Chen, H., Zhang, C., Emmelin, C., Chen, J., George, C.,
141   and Wang, L.: Chemical Characteristics of Organic Aerosols in Shanghai: A Study by Ultrahigh-
142   Performance Liquid Chromatography Coupled With Orbitrap Mass Spectrometry, J. Geophys. Res.
143   Atmos., 122, 11,703-11,722, https://doi.org/10.1002/2017JD026930, 2017.

144   Yassine, M. M., Harir, M., Dabek-Zlotorzynska, E., and Schmitt-Kopplin, P.: Structural characterization
145   of organic aerosol using Fourier transform ion cyclotron resonance mass spectrometry: aromaticity
146   equivalent   approach,   Rapid   Commun.   Mass   Spectrom.,   28,   2445–2454,
147   https://doi.org/10.1002/rcm.7038, 2014.

148   Ye, C., Yuan, B., Lin, Y., Wang, Z., Hu, W., Li, T., Chen, W., Wu, C., Wang, C., Huang, S., Qi, J., Wang,
149   B., Wang, C., Song, W., Wang, X., Zheng, E., Krechmer, J. E., Ye, P., Zhang, Z., Wang, X., Worsnop,
150   D. R., and Shao, M.: Chemical characterization of oxygenated organic compounds in the gas phase
151   and particle phase using iodide CIMS with FIGAERO in urban air, Atmos. Chem. Phys., 21, 8455–
152   8478, https://doi.org/10.5194/acp-21-8455-2021, 2021.

153   Yu, S. S., Jia, L., Xu, Y. F., and Pan, Y. P.: Molecular composition of secondary organic aerosol from
154   styrene   under   different   NOx   and   humidity   conditions,   Atmos.   Res.,   266,   105950,
155   https://doi.org/10.1016/j.atmosres.2021.105950, 2022.

156